

Suppression of the Rhines effect and the location of vortices on Saturn

A. B. Penny,¹ A. P. Showman,² and D. S. Choi²

Received 21 March 2009; revised 14 September 2009; accepted 28 September 2009; published 16 February 2010.

[1] Saturn's atmosphere contains numerous vortices that reside predominantly within specific localized latitude bands. Two-dimensional turbulence theory predicts that vortices which do form are readily destroyed as they interact with dispersive Rossby waves in a process called the "Rhines effect," which acts to organize turbulent energy into alternating zonal flows through the interaction of Rossby waves and turbulence of similar scales. Observations show that at some latitudes, vortices are more prevalent, suggesting that Rossby waves are suppressed in these regions. Following the method applied to Jupiter by Theiss (2006), we generalize the 2-D Rhines scale to include depth-dependent flow with a finite deformation radius; this allows for a simple estimate of the conditions under which Rossby waves are suppressed in the cloud layer. We then compare the latitudes of known vortices to the predicted latitudes where Rossby waves may be suppressed on Saturn. We find a good correlation, suggesting that, as on Jupiter, Rossby wave suppression helps explain the prevalence of vortices at specific latitudes on Saturn.

Citation: Penny, A. B., A. P. Showman, and D. S. Choi (2010), Suppression of the Rhines effect and the location of vortices on Saturn, *J. Geophys. Res.*, 115, E02001, doi:10.1029/2009JE003384.

1. Introduction

[2] Like other gas giant planets, Saturn has a turbulent atmosphere containing numerous vortices (Figure 1). The large-scale circulation pattern on Saturn exhibits about 10 zonal jets each in the northern and southern hemispheres that are nearly symmetric about a strong prograde (eastward) jet at the equator that peaks in velocity near 470 m s^{-1} [Smith *et al.*, 1981, 1982; Sánchez-Lavega *et al.*, 2000; Vasavada *et al.*, 2006; Choi *et al.*, 2009].

[3] In an effort to describe the process responsible for forming such alternating zonal jets, Rhines [1975] realized that the gradient of planetary vorticity can be responsible for the growth of disturbances in the east-west direction relative to the north-south direction, as Rossby waves interact with turbulence to induce alternating zonal flows. Theiss [2006] noted that interaction with dispersive Rossby waves will act to deform and eventually destroy any vortices that are embedded in the flow. However, observations show that vortices tend to cluster at specific latitudes, and assuming that the time scales for vortex formation are much longer than those over which Rossby wave dispersion would act to destroy the vortices, it suggests that there are certain locations where Rossby waves are suppressed. Theiss [2006] proposed that a formulation of the Rhines effect to include baroclinic modes (depth-dependent flow) can allow for the suppression of the Rhines effect when certain criteria are met and found

that the location of vortices on Jupiter correlate well with the latitudes where the Rhines effect appears to be suppressed.

[4] Here, we extend the analysis of Theiss [2006] to Saturn. Our study relies on recent analyses of Cassini data, both imaging science subsystem (ISS) [Vasavada *et al.*, 2006] and visual infrared mapping spectrometer (VIMS) [Choi *et al.*, 2009], which have provided insight into the complex nature of the flow below Saturn's cloud layer (Figure 1). VIMS is able to see features below the relatively featureless haze layer (through the $5 \mu\text{m}$ window) which are backlit by Saturn's thermal emission [Choi *et al.*, 2009], while ISS observes reflected solar irradiance within the ultraviolet to near-infrared wavelength range [Vasavada *et al.*, 2006].

[5] By comparing the Voyager 1 and 2 zonal wind profile data from Sánchez-Lavega *et al.* [2000] with the recent cloud-feature spot count from Choi *et al.* [2009] obtained from a combination of VIMS data and an analysis of ISS data by Vasavada *et al.* [2006], this paper expands upon the method introduced by Theiss [2006] by applying his modified Rhines scale to Saturn to determine whether latitudes predicted to be favorable for Rossby wave suppression correspond to the latitudes of observed vortices. Further expanding on the approach used by Theiss [2006], in which the deformation radius is a specified function of latitude and the deep flow is assumed to be zero, we include the possibility of a nontrivial deep layer flow and a deformation radius that can be adjusted as a free parameter.

[6] We make the assumption that spots observed in the VIMS data by Choi *et al.* [2009] are vortices, although no direct detection of spot vorticity was reported in their study due to resolution limitations. However, there is evidence to support this assumption as latitudes containing vortices in the detailed ISS vortex count of Saturn's southern hemisphere by Vasavada *et al.* [2006] match closely latitudes where

¹Department of Atmospheric Sciences, University of Arizona, Tucson, Arizona, USA.

²Department of Planetary Sciences, University of Arizona, Tucson, Arizona, USA.

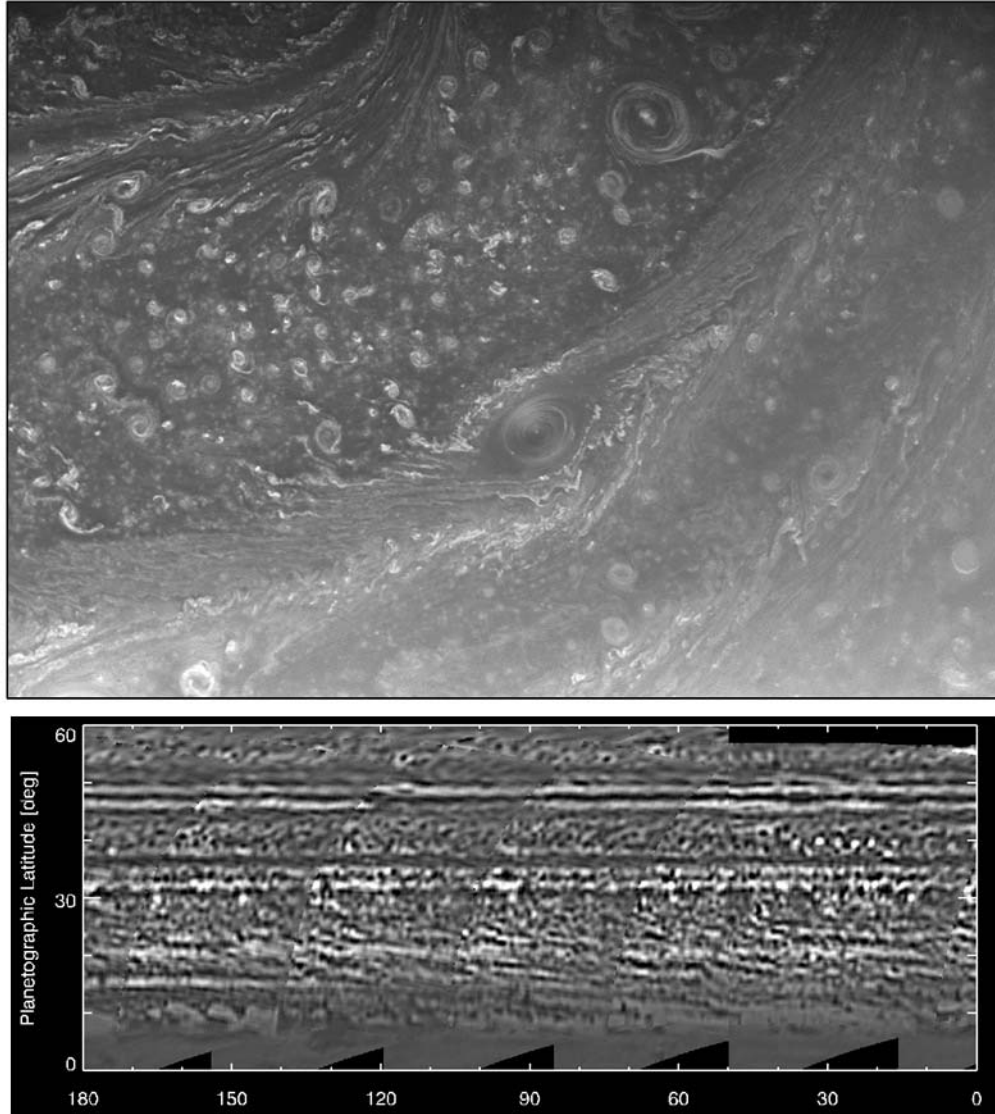


Figure 1. (top) ISS infrared image (centered at 752 nm) of vortices along a turbulent region near 70°N (courtesy NASA, JPL, Space Science Institute). Saturn’s north polar hexagon is visible in the upper left of the image. (bottom) VIMS northern hemisphere mosaic as observed at 5 μm used to derive the spot count analyzed in this study [Choi *et al.*, 2009]. The northern hemisphere VIMS mosaic was constructed from images taken in September 2006.

Choi *et al.* [2009] have identified spots from VIMS data, even though the number of spots per latitude far exceeds the number of identified vortices. In addition, our choice of including the analysis of VIMS data by Choi *et al.* [2009] allows for a nearly global comparison of vortex latitudes to the latitudes where we consider the Rhines effect to be suppressed. Nevertheless, we have no direct evidence for the vortical nature of the circular features; higher resolution observations by Cassini ISS or instruments on a future spacecraft will be needed to confirm this.

2. Rhines Effect and Its Suppression

[7] To determine under what conditions the Rhines effect may be suppressed, we first begin by assuming the flow to be depth-independent, or 2-D, and later extend the model to

be depth-dependent by including a finite deformation radius. Thus, the nondivergent, 2-D potential vorticity equation on a β plane is

$$\frac{\partial \zeta}{\partial t} + \vec{v} \cdot \vec{\nabla} \zeta + \beta v = 0, \quad (1)$$

where ζ is the relative vorticity, \vec{v} is the horizontal wind, $\vec{\nabla} \zeta$ is the horizontal gradient of relative vorticity, v is the meridional wind speed, and $\beta = \partial f / \partial y$ is the gradient of planetary vorticity, where $f = 2\Omega \sin \phi$ is the Coriolis parameter, Ω is the planetary rotation rate, and ϕ is the latitude. Two different flow regimes are possible depending on the relative magnitudes of the nonlinear advection term ($\vec{v} \cdot \vec{\nabla} \zeta$) and β term (βv) from equation (1). When the nonlinear advection term dominates, the flow is generally characterized by turbulence,

and when the β term dominates, Rossby waves are generated [Vallis, 2006].

[8] To illustrate these two regimes, in neglecting the non-linear advection term from equation (1), the Rossby wave frequency can be expressed as

$$\omega_r = \frac{-\beta k_x}{k_x^2 + k_y^2} = \frac{-\beta \cos \alpha}{|\vec{k}|}, \quad (2)$$

where k_x and k_y are the zonal and meridional wave numbers of the Rossby wave, respectively, $|\vec{k}|$ is the total wave number magnitude ($\sqrt{k_x^2 + k_y^2}$), and α is the angle between the direction of wave propagation and east [Vasavada and Showman, 2005]. If one then equates the Rossby frequency, ω_r , with the characteristic turbulence frequency $\omega_t = U_{\text{rms}} |\vec{k}|$, where U_{rms} is taken to be the typical eddy-scale velocity, one obtains

$$k_\beta^2 = \frac{\beta}{U_{\text{rms}}} |\cos \alpha|, \quad (3)$$

thus arriving at the Rhines scale, following Rhines [1975], where k_β is the critical wave number magnitude (as a function of α) where the inverse energy cascade slows an energy tends to accumulate. In the standard picture, scales with $|\vec{k}| < k_\beta$ are associated with Rossby waves and scales with $|\vec{k}| > k_\beta$ are associated with turbulence (but see Sukoriansky *et al.* [2007]). Because the Rhines scale is anisotropic (i.e., k_β depends on α), energy reaching wave number magnitudes of $\sim \beta/U_{\text{rms}}$ tends to organize into alternating zonal flows with a characteristic length scale of $L_\beta \approx \pi/k_\beta$ [Vasavada and Showman, 2005].

[9] Similar to the method outlined by Theiss [2006], we followed the formulation of Okuno and Masuda [2003] to generalize to a depth-dependent flow by introducing a finite deformation radius such that the Rossby wave dispersion relation modifies to

$$\omega_r = \frac{-\beta k_x}{k_x^2 + k_y^2 + L_D^{-2}}, \quad (4)$$

where k_x and k_y are again the zonal and meridional wave numbers of the Rossby wave, respectively, and L_D is the deformation radius [Showman, 2007]. This leads to an altered Rhines scale of

$$k_\beta^2 = \frac{\beta}{U_{\text{rms}}} |\cos \alpha| - L_D^{-2}, \quad (5)$$

where for a small enough deformation radius the Rhines scale goes to zero for all values of α and the Rhines effect is suppressed such that the entire wave number space is dominated by turbulence. This allows the frequency scale of the turbulence to be larger than that for Rossby waves at every wave number, which inhibits their interaction and prevents vortices embedded in the turbulence from being destroyed by Rossby waves [Okuno and Masuda, 2003; Smith, 2004; Vasavada and Showman, 2005; Theiss, 2006].

[10] A finite deformation radius and the presence of a mean flow affect the potential vorticity gradient. We include these effects as follows:

$$\beta^* = \beta - \frac{\partial^2 \bar{u}}{\partial y^2} + \frac{\bar{u} - \bar{u}_{\text{deep}}}{L_D^2} \quad (6)$$

[Lipps, 1963], where \bar{u} is the mean zonal wind at cloud level, \bar{u}_{deep} is the ‘‘deep’’ mean zonal wind, y is northward distance, and $\partial^2 \bar{u}/\partial y^2$ is the curvature of the mean zonal wind with northward distance at cloud level. Evident from equation (4), $|\beta^*| |\vec{k}| L_D^2$ can be considered an upper bound for the Rossby wave frequency (the phase speed of the long Rossby wave limit where $|\vec{k}| \rightarrow 0$) such that one can compute a criterion for the suppression of the Rhines effect by allowing the turbulence frequency to exceed the Rossby wave upper limit. Thus, when $\omega_t > |\beta^*| |\vec{k}| L_D^2$, the Rhines effect is suppressed. After expressing the turbulence frequency as $\omega_t = U_{\text{rms}} |\vec{k}|$, suppression of the Rhines effect occurs when the eddy-scale velocity exceeds the defined critical velocity, U_c , as

$$U_{\text{rms}} > U_c = |\beta^*| L_D^2. \quad (7)$$

[11] What is the relationship between this criterion and the more-familiar Charney–Stern criterion governing the stability of zonal jets? For a one-layer fluid, the Charney–Stern stability criterion states that zonally symmetric zonal jets are stable when the gradient of potential vorticity with latitude (given in the quasi-geostrophic one-layer model by β^*) does not change sign within the domain [Dowling, 1995b]. Since we expect that β^* must be positive somewhere, the criterion would require that $\beta^* \geq 0$ everywhere. Thus, the two criteria differ significantly: equation (7) is a criterion for flow behavior depending on the value of U_{rms} (relative to the value of β^*) whereas Charney–Stern provides information on jet stability depending on the sign of β^* . When a flow is neutral with respect to the Charney–Stern stability criterion (i.e., when $\beta^* = 0$), then according to (7) the Rhines effect is always suppressed. This results from the fact that when the mean potential vorticity gradient is zero (i.e., $\beta^* = 0$), Rossby waves cannot exist and hence cannot cause dispersion of coherent vortices. However, the reverse is not true: suppression of the Rhines effect does not require neutrality with respect to the Charney–Stern criterion. When a flow is stable with respect to the Charney–Stern criterion ($\beta^* > 0$ everywhere), the Rhines effect can be suppressed when turbulence velocities are large but would not be suppressed when turbulence velocities are small. In this situation, the flow is capable of supporting Rossby waves, but (according to the frequency-matching argument given above) they will interact with the turbulence only when the turbulence velocities are sufficiently small. In this case, sufficiently large turbulence velocities will prevent energy transfer into Rossby waves, thereby inhibiting the dispersion of coherent vortices despite the fact that the latitudinal potential vorticity gradient is nonzero.

3. Method for Calculating U_c for Saturn

[12] In order to calculate U_c for Saturn, we obtained the latitudinal profile of the zonal winds and the eddy-scale

velocity from the recent analysis of Voyager 1 and 2 data by *Sánchez-Lavega et al.* [2000]. The second derivative of the zonal jets with respect to northward distance ($\partial^2\bar{u}/\partial y^2$) was calculated by first finding the change in northward distance with respect to planetographic latitude ($dy/d\phi_g$) at intermediate points between observations following *Dowling et al.* [1998]:

$$\frac{dy}{d\phi_g} = \frac{r(\phi_g)/\cos\phi_g}{\sin^2\phi_g + (R_e/R_p)^2\cos^2\phi_g}, \quad (8)$$

where ϕ_g is the planetographic latitude, $r(\phi_g) = R_e/(1 + (R_p/R_e)^2\tan^2\phi_g)^{1/2}$ is the zonal radii of curvature, and R_e and R_p are Saturn's equatorial and polar radii (60,268 km and 54,364 km, respectively). We then calculated the second derivative of the zonal jets with respect to northward distance using a centered second-order finite difference scheme which allows for varying Δy and takes the following form (here calculated for a central observation point denoted by subscript 1):

$$\left(\frac{d^2\bar{u}}{dy^2}\right)_1 = \frac{\bar{u}_2 - \bar{u}_1}{\frac{1}{2}\Delta y_b(\Delta y_a + \Delta y_b)} - \frac{\bar{u}_1 - \bar{u}_0}{\frac{1}{2}\Delta y_a(\Delta y_a + \Delta y_b)}, \quad (9)$$

where \bar{u} is the observed mean zonal wind and $\Delta y_a = (dy/d\phi_g)\Delta\phi_g$ is the change in northward distance between observations \bar{u}_0 and \bar{u}_1 , with $\Delta\phi_g$ being the difference in planetographic latitude and $dy/d\phi_g$ calculated midway between observations. Similarly, Δy_b is the change in northward distance between observations \bar{u}_1 and \bar{u}_2 . A $\sim 2.5^\circ$ running average was then used to smooth $\partial^2\bar{u}/\partial y^2$ in an effort to remove sensitivities to small fluctuations in the data.

[13] The gradient of planetary vorticity in equation (6) was computed as follows: $\beta = df/dy = (df/d\phi_g)(d\phi_g/dy) = 2\Omega \cos\phi_g(d\phi_g/dy)$, where Ω is the angular rotation rate of Saturn (taken to be $1.63784 \times 10^{-4} \text{ s}^{-1}$), and $d\phi_g/dy$ is computed from the inverse of equation (8). The depth-dependent flow term $(\bar{u} - \bar{u}_{\text{deep}})L_D^2$ in equation (6) involves the deformation radius which was treated as a free parameter. Instead of allowing the “deep” flow to simply vanish ($\bar{u}_{\text{deep}} \rightarrow 0$), as *Theiss* [2006] assumed, our model allows for \bar{u}_{deep} to be nonzero in an attempt to see how the mean flow below the cloud layer might affect the suppression of the Rhines effect.

4. Results and Discussion

[14] As shown in section 3, we utilized the mean zonal wind profile from *Sánchez-Lavega et al.* [2000] to compute U_c as a function of latitude and compared this to the U_{rms} also from their study. Figure 2 reveals latitudes where the Rhines effect is suppressed ($U_c < U_{\text{rms}}$) and compares these areas with the latitudinal profile of spots (vortices) analyzed by *Choi et al.* [2009]. Here the “deep” flow (\bar{u}_{deep}) is zero and the deformation radius (L_D) follows a simplified $1\frac{1}{2}$ -layer formulation as $L_D = \sqrt{gH}/f$, where again f is the Coriolis parameter, g is the gravitational acceleration (taken as a constant at 10.4 m s^{-2}), and here we assume H to be the scale height evaluated using a temperature of 134 K and a specific gas constant of $3700 \text{ J kg}^{-1} \text{ K}^{-1}$. It should be noted that the scale height H should be considered to be a function

of latitude under baroclinic flow ($\bar{u}_{\text{deep}} \neq \bar{u}$), but in the quasi-geostrophic regime we expect fractional variations of H to be small, and here we make the simplifying assumption that H is constant with latitude.

[15] Although the criterion of $U_c < U_{\text{rms}}$ is not satisfied at all locations where vortices are identified from VIMS and ISS observations, a broad correlation is immediately evident from Figure 2. Note from Figure 1 that VIMS vortex counts were not available north of 60°N to compare with the predicted band of Rossby wave suppression near 72°N shown in Figure 2. Apparent from the left plot of Figure 2 is that several distinct bands of vortices exist (near 55°N , 40°N , 42°S , 55°S , and 65°S). At all five latitudes where clusters of vortices have been identified, the Rhines effect is suppressed according to our criterion (denoted by black asterisks). Between 38.5°S and 46°S , an abundance of vortices exists, helping to give this region the name “storm alley” [*Vasavada et al.*, 2006], and the Rhines effect is shown to be suppressed or very nearly suppressed over the same range of latitudes.

[16] We believe that the areas where the criterion is not satisfied but is relatively close to being so may still be significant, as the broad spatial pattern of observed vortices seems to match well with these slightly sub-critical regions, especially considering that there is a great deal of uncertainty in both U_{rms} and U_c . The latitudinal profile of U_{rms} calculated by *Sánchez-Lavega et al.* [2000] contains both fluctuations of the mean zonal wind as well as observational errors due to image navigation and uncertainty from cloud-feature identification. Since it is not possible to isolate the eddy velocity from the observational errors, we consider U_{rms} to be an upper bound on the eddy velocity. The largest degree of uncertainty in calculating the suppression criterion arises from our assumption of values for L_D and \bar{u}_{deep} which are important factors in calculating β^* in equation (6), and ultimately in determining U_c , and were therefore treated as free parameters. Furthermore, it is also worth mentioning that actual values of U_c may be less than those computed, as equation (7) relies on the upper bound of the Rossby wave frequency.

[17] It is important to note that nearly 30 years have elapsed since the zonal wind profile of Saturn was observed by Voyagers 1 and 2. Comparing this profile to the recent VIMS and ISS analyses forces the assumption that the zonal winds and eddy velocity magnitudes have not evolved over this time. This assumption may not be true and could have a negative effect on the correlation of the results.

[18] In an effort to determine how the magnitude of U_c can be reduced so that $U_c < U_{\text{rms}}$, it is evident from equation (7) that $U_c < U_{\text{rms}}$ when $\beta^* \rightarrow 0$. Equation (7) can be expanded, and as a result of the $|\beta^*|$ factor, two solutions are possible depending on the sign and magnitude of $\partial^2\bar{u}/\partial y^2$. If $\beta^* > 0$, U_c takes the form from (6) and (7) as

$$U_c = \beta L_D^2 - \frac{\partial^2\bar{u}}{\partial y^2} L_D^2 + (\bar{u} - \bar{u}_{\text{deep}}). \quad (10)$$

Comparing Figures 2 and 3 (which shows the latitudinal profile of the terms comprising U_c) reveals that a preferred location for the suppression of the Rhines effect exists where $\partial^2\bar{u}/\partial y^2 > 0$. This generally occurs near minima in eastward

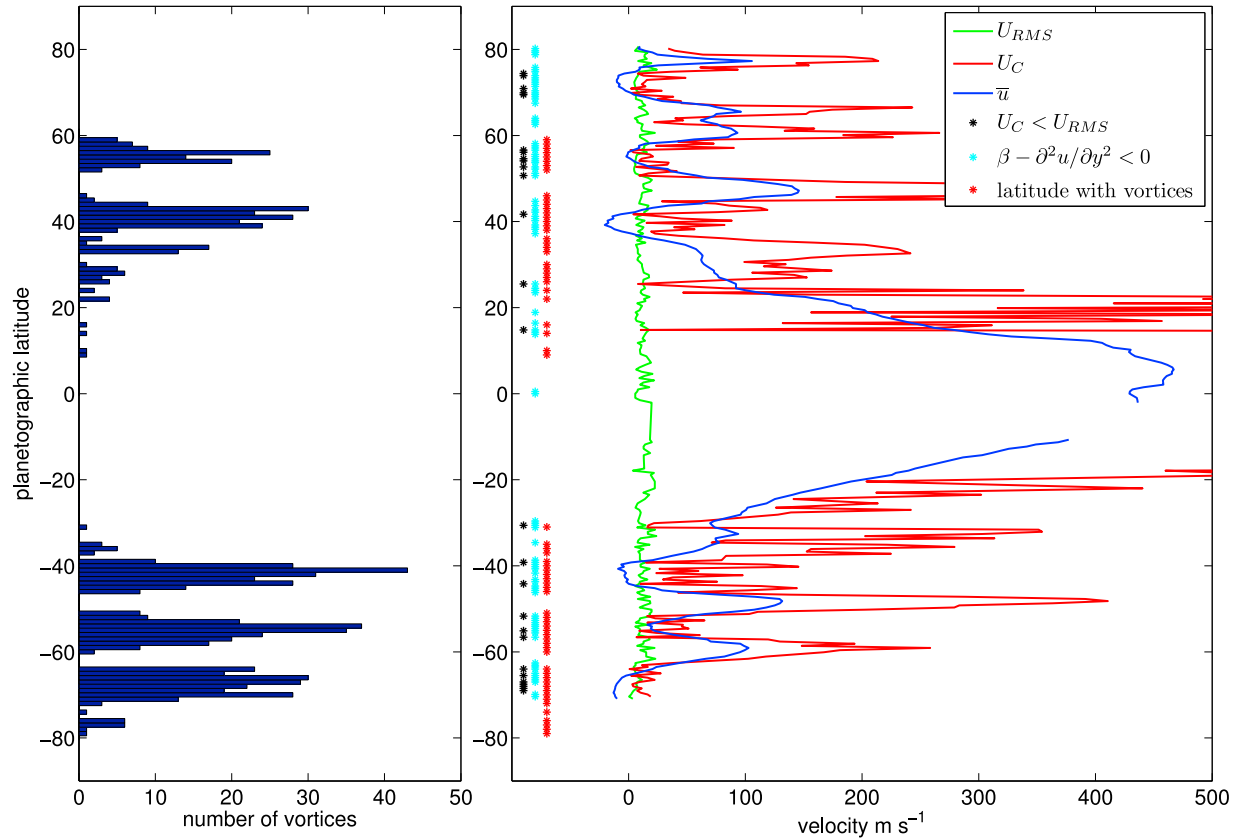


Figure 2. (left) Number of vortices as a function of latitude observed by VIMS and ISS [Choi *et al.*, 2009] (right) compared with locations where the Rhines effect should be suppressed as calculated from the zonal wind profile analyzed by Sánchez-Lavega *et al.* [2000]. The mean zonal wind profile is blue, the eddy-scale velocity is green, and the critical velocity is red. Black asterisks denote latitudes where the Rhines effect is suppressed, blue asterisks indicate regions where the 2-D barotropic stability criterion is violated, and red asterisks depict latitudes where vortices are observed in the VIMS and ISS data sets. Here $\bar{u}_{\text{deep}} = 0$ and the deformation radius follows \sqrt{gH}/f , where g is the gravitational acceleration, H is the scale height, and f is the Coriolis parameter.

wind velocities or near westward jets depending on assumptions made about Saturn’s rotation rate [Sánchez-Lavega, 2005; Anderson and Schubert, 2007]. In addition, this also coincides with locations where the depth-dependent flow term of equation (6) approaches zero as \bar{u} is relatively small in magnitude near the westward jets. Thus the westward jets provide an area where the depth-dependent flow term is small and the curvature of the mean winds is positive, necessitating that β^* approach zero at these locations, allowing the Rhines effect to be suppressed.

[19] In their analysis of ISS data, Vasavada *et al.* [2006] also show that Saturnian vortices tend to exist near westward jets or favor latitude regions where the curvature of the zonal winds is positive and exceeds the gradient of planetary vorticity, namely where the barotropic stability criterion is violated (denoted by the light blue asterisks in Figure 2). It is therefore tempting to try to explain the existence of vortices in these regions in terms of barotropic stability. However, simply attributing the presence of vortices at certain latitudes to be a consequence of 2-D shear stability remains problematic for two reasons. First, there is doubt whether the 2-D stability criterion is relevant for explaining the dynamics in 3-D atmospheres. This is illustrated by the

fact that the region exhibiting the most vortices on Saturn (near 40°S) violates the barotropic stability criterion the least [Vasavada *et al.*, 2006], and at certain locations on both Jupiter and Saturn where observations show cloud-level jets to be stable, they are in strong violation of the shear stability criterion [Dowling, 1995a]. Second, even if the westward jets are unstable, maintaining high vortex populations cannot be attributed solely to having an unstable jet profile, as Rossby wave dispersion will act to destroy vortices in a matter of days without some ameliorating factor to amplify vortex lifetime. (A vortex can be viewed as a Rossby wave packet with zonal wave numbers spanning some width Δk around a central value k_x , and generally we expect $\Delta k \sim k_x$. VIMS and ISS images contain numerous small spots, which are assumed to be vortices, with sizes $\sim 1000\text{--}2000$ km, presumably similar to the radius of deformation. Assuming $\Delta k \sim k_x \sim 1/L_D$, the Rossby wave dispersion relation (equation (4)) then suggests that the range of Rossby waves a vortex can radiate will have phase speeds differing by order unity, namely ~ 10 m s $^{-1}$ for Saturn’s midlatitude value of β and L_D (~ 2000 km). This suggests a vortex dispersion time of a few days.) Note that nonlinearity can counteract vortex dispersion but fails to describe the latitude dependence of

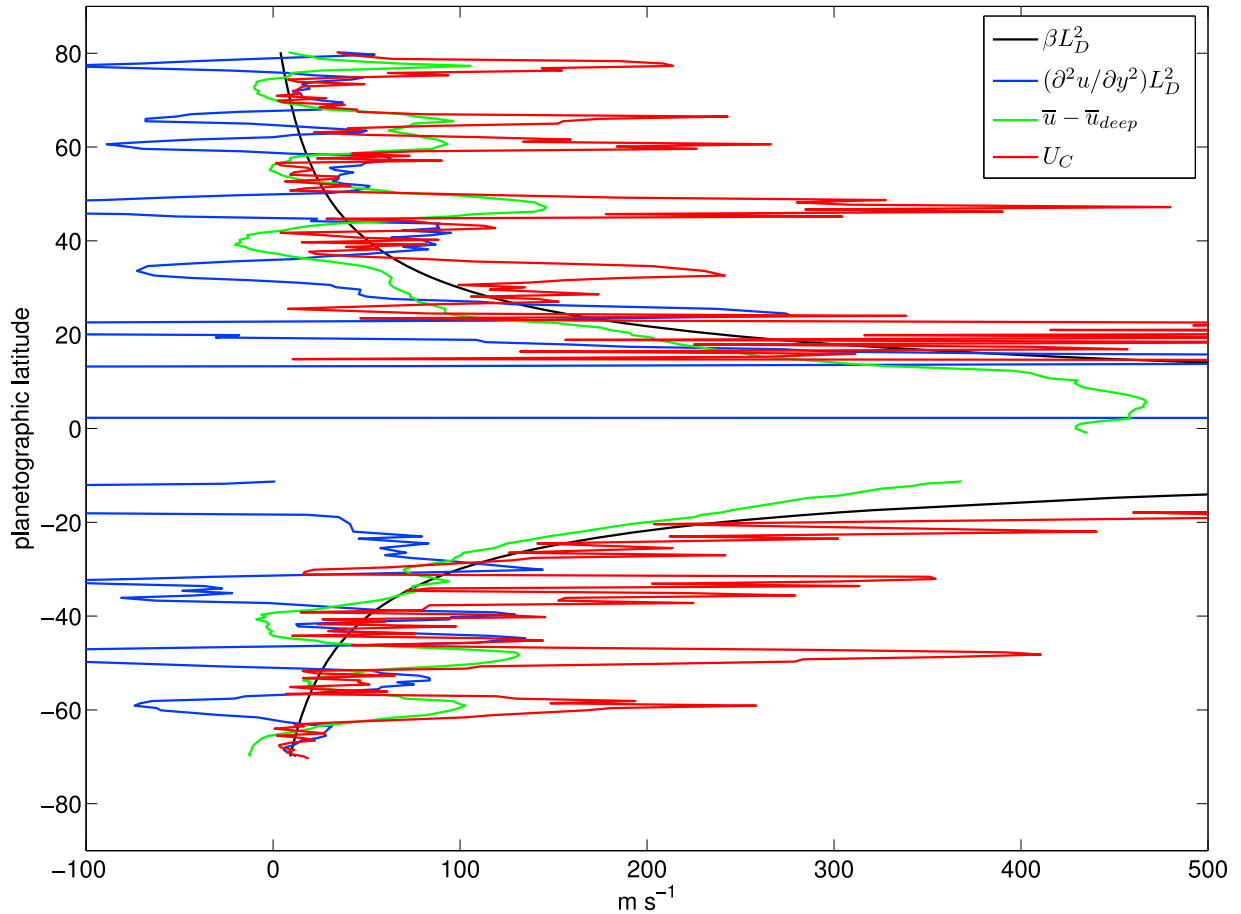


Figure 3. Magnitude of various terms comprising U_c . Black represents the first term of equation (10), blue the second, green the third, and U_c is colored in red. Here $\bar{u}_{\text{deep}} = 0$ and the deformation radius follows \sqrt{gH}/f , where g is the gravitational acceleration, H is the scale height, and f is the Coriolis parameter.

the vortex population. Since the jets are pumped up gradually (a result of Saturn’s low heat flux), it follows that vortex formation occurs as an intermittent process, over much longer time scales than required for vortex destruction in the presence of dispersive Rossby waves. This suggests that other processes, such as the suppression of Rossby wave interaction with the vortices, are important in determining where vortices exist.

[20] Somewhat in contrast to what was noted for Jupiter by *Theiss* [2006], there does not appear to be a general increase in the width of the regions where the Rhines effect is suppressed poleward of 40° latitude on Saturn. This may explain why Saturn does not share the same obvious increase in the number of vortices with latitude observed on Jupiter [*Vasavada et al.*, 2006] and could in part be due to the much stronger zonal flow on Saturn compared to Jupiter. We can see from Figure 3 that with increasing latitude, $\beta L_D^2 \rightarrow 0$ in a similar fashion as it does for Jupiter [*Theiss*, 2006]. However, the jets on Saturn reach velocities two to three times that on Jupiter poleward of 40° latitude, suggesting that the other two terms in equation (10) play a more important role for Saturn than Jupiter in determining the value of U_c and ultimately where the Rhines effect is suppressed at higher latitudes.

[21] Several parameters were varied in order to check the sensitivity of the criterion. The deep flow (\bar{u}_{deep}) was set to various factors of \bar{u} (0.5, 1.0, and 2.0). When the deep flow was set equal to 0.5 \bar{u} (not shown), no significant changes occurred in the latitudes where the Rhines effect is suppressed. In a recent modeling study, *García-Melendo et al.* [2007] conducted several simulations of Saturn’s “Brown Spot” (BS), which is an anticyclonic vortex located at 43°N , in which the static stability and vertical profile of the zonal wind were allowed to vary. By tuning these model parameters until the simulated drift velocity of BS matched observations, *García-Melendo et al.* [2007] found that the vertical gradient of the mean zonal wind ($\partial\bar{u}/\partial z$) was relatively small, suggesting that $\bar{u}_{\text{deep}} \approx \bar{u}$ near the location of Saturn’s BS. Setting the deep flow equal to the flow at the cloud level allows $\beta^* \rightarrow 0$ at locations where the depth-dependent flow term was otherwise relatively large (see Figure 3), allowing U_c to become smaller and thus approach U_{rms} over a wider latitude range, especially away from the equator. However, similar to the 0.5 \bar{u} case, this fails to improve upon the correlation that exists with no deep flow. When the deep flow is of greater magnitude than the cloud level flow, U_c is comparable to U_{rms} over nearly the entire region poleward of 20° latitude, but again, the overall agreement is not improved compared with the zero deep flow case shown in Figure 2.

[22] Motivated by uncertainty in the actual rotation rate of Saturn [Sánchez-Lavega, 2005; Anderson and Schubert, 2007], we also tried reducing the zonal wind profile from Sánchez-Lavega et al. [2000] by 20 m s^{-1} across all latitudes. The overall pattern of U_c in this case is quite similar to that shown in Figure 2, except that U_c becomes much larger than U_{rms} at higher latitudes.

[23] The deformation radius L_D was also allowed to vary from the simplified $1\frac{1}{2}$ -layer formulation discussed earlier. In their study of Saturn's BS, García-Melendo et al. [2007] estimated that $L_D \approx 2200 \text{ km}$ within the “weather layer” near the latitude of BS. In another study by Read et al. [2009], temperature measurements from the Cassini composite infrared spectrometer (CIRS) were used in conjunction with wind velocities derived from cloud-tracking to obtain an estimate of the latitudinal profile of L_D by using Arnol'd's second stability theorem as an additional constraint. Values of L_D from the best fit latitudinal profile calculated by Read et al. [2009] are smaller in magnitude than those obtained from the simplified $1\frac{1}{2}$ -layer formulation, but seem to agree very closely with what is suggested from the study by García-Melendo et al. [2007] for the latitude region near 43°N . The L_D profile from Read et al. [2009] was therefore used in this study to see if our correlation could be improved upon. Although a better agreement was found at higher latitudes, the correlation between vortex locations and latitudes where $U_c < U_{\text{rms}}$ was not as strong equatorward of 40° latitude compared with the results obtained from the simplified $1\frac{1}{2}$ -layer formulation.

[24] Another interesting result evident from Figure 2 is that there is a noticeable absence of vortices at latitudes where the Rossby wave suppression criterion is not satisfied ($U_c > U_{\text{rms}}$), such as near peaks of eastward jets, including the equatorial jet. In addition, notable features such as the “Ribbon” at 46°N [Godfrey and Moore, 1986; Sánchez-Lavega, 2002], Saturn's polar hexagon near 78°N [Godfrey, 1988; Allison et al., 1990; Sánchez-Lavega et al., 1993; Fletcher et al., 2008], and waves identified at 32°S and 48°S [Sánchez-Lavega et al., 2000], all of which appear to be types of Rossby waves, exist at latitudes where our criterion is not satisfied. The lack of vortices at latitudes where wave-like features are present suggests that the suppression of the Rhines effect is not only an important factor in determining where vortices are likely to exist, but it may also explain why Rossby wave-type features are more prominent at certain latitudes where vortices are generally absent.

5. Summary

[25] A scheme analogous to the approach of Theiss [2006] for Jupiter was applied to Saturn to determine whether latitudes where vortices exist match latitudes where the Rhines effect might be suppressed. When the Rhines effect is suppressed, Rossby waves are inhibited from interacting with turbulence, and vortices, if present, are prevented from being deformed and eventually destroyed. We found that latitudes which display a local maximum in the number of circular vortex-like features, as observed recently by Cassini ISS [Vasavada et al., 2006] and VIMS [Choi et al., 2009], seem to correspond well with latitudes where the Rhines effect is suppressed or nearly suppressed. Several parameters

were varied in an effort to see whether the correlation could be improved, namely the presence of a nonzero deep-level flow, a varying deformation radius, and a reduction in the zonal wind profile due to some uncertainty of Saturn's rotation rate, but none of these changes seemed to yield a better agreement. The results presented here for Saturn complement the findings of Theiss [2006] for Jupiter and suggest that the suppression of the Rhines effect is an important criterion in determining where persistent vortices are likely to exist. Although a precise one-to-one relationship is not observed between latitudes of predicted Rhines effect suppression and latitudes of observed vortices, the general trends show good agreement, especially considering the high degree of uncertainty involved in calculating the suppression criterion and the fact that the data sets used in this analysis span a significant period of time. With additional modeling studies and more detailed observations, further analyses evaluating the suppression of the Rhines effect can be conducted, which will help to improve our understanding of the turbulent atmospheres of Jupiter and Saturn.

[26] **Acknowledgments.** The authors would like to thank the two anonymous reviewers for their insightful and constructive comments that greatly improved the manuscript. This project was supported by NASA Planetary Atmosphere grants NNG06GF28G and NNX07AF35G to A.P.S. and was made possible in part by a Science Foundation Arizona graduate research fellowship.

References

- Allison, M., D. A. Godfrey, and R. F. Beebe (1990), A wave dynamical interpretation of Saturn's polar hexagon, *Science*, *247*, 1061–1063.
- Anderson, J. D., and G. Schubert (2007), Saturn's gravitational field, internal rotation, and interior structure, *Science*, *317*, 1384–1387.
- Choi, D. S., A. P. Showman, and R. H. Brown (2009), Cloud features and zonal wind measurements of Saturn's atmosphere as observed by Cassini/VIMS, *J. Geophys. Res.*, *114*, E04007, 10.1029/2008JE003254.
- Dowling, T. E. (1995a), Estimate of Jupiter's deep zonal-wind profile from Shoemaker-Levy 9 data and Arnol'd's second stability criterion, *Icarus*, *117*, 439–442.
- Dowling, T. E. (1995b), Dynamics of Jovian atmospheres, *Annu. Rev. Fluid Mech.*, *27*, 293–334.
- Dowling, T. E., A. S. Fischer, P. J. Gierasch, J. Harrington, R. P. LeBeau Jr., and C. M. Santori (1998), The Explicit Planetary Isentropic-Coordinate (EPIC) atmospheric model, *Icarus*, *132*, 221–238.
- Fletcher, L. N., et al. (2008), Temperature and composition of Saturn's polar hot spots and hexagon, *Science*, *319*, 79–81, doi:10.1126/science.1149514.
- García-Melendo, E., A. Sánchez-Lavega, and R. Hueso (2007), Numerical models of Saturn's long-lived anticyclones, *Icarus*, *191*, 665–677.
- Godfrey, D. A. (1988), A hexagonal feature around Saturn's north pole, *Icarus*, *76*, 335–356.
- Godfrey, D. A., and V. Moore (1986), The Saturnian ribbon feature: A baroclinically unstable model, *Icarus*, *68*, 314–343.
- Lipps, F. (1963), Stability of jets in a divergent barotropic fluid, *J. Atmos. Sci.*, *20*, 120–129.
- Okuno, A., and A. Masuda (2003), Effect of horizontal divergence on the geostrophic turbulence on a beta-plane: Suppression of the Rhines effect, *Phys. Fluids*, *15*, 13–48.
- Read, P. L., B. J. Conrath, L. N. Fletcher, P. J. Gierasch, A. A. Simon-Miller, and L. C. Zuchowski (2009), Mapping potential vorticity dynamics on Saturn: Zonal mean circulation from Cassini and Voyager data, *Planet. Space Sci.*, *57*, 1682, 10.1016/j.pss.2009.03.004.
- Rhines, P. B. (1975), Waves and turbulence on a beta-plane, *J. Fluid Mech.*, *69*, 417–443.
- Sánchez-Lavega, A. (2002), Observations of Saturn's ribbon wave 14 years after its discovery, *Icarus*, *158*, 272–275, doi:10.1006/icar.2002.6864.
- Sánchez-Lavega, A. (2005), How long is the day on Saturn?, *Science*, *307*, 1223–1224.
- Sánchez-Lavega, A., J. Lecacheux, F. Colas, and P. Laques (1993), Ground-based observations of Saturn's north polar spot and hexagon, *Science*, *260*, 329–332.
- Sánchez-Lavega, A., J. F. Rojas, and P. V. Sada (2000), Saturn's zonal winds at cloud level, *Icarus*, *147*, 405–420.

- Showman, A. P. (2007), Numerical simulations of forced shallow-water turbulence: Effects of moist convection on the large-scale circulation of Jupiter and Saturn, *J. Atmos. Sci.*, *64*, 3132–3157.
- Smith, B. A., et al. (1981), Encounter with Saturn: Voyager 1 imaging science results, *Science*, *212*, 163–191.
- Smith, B. A., et al. (1982), A new look at the Saturn system: The Voyager 2 images, *Science*, *215*, 504–537.
- Smith, K. S. (2004), A local model for planetary atmospheres forced by small-scale convection, *J. Atmos. Sci.*, *61*, 1420–1433.
- Sukoriansky, S., N. Dikovskaya, and B. Galperin (2007), On the arrest of inverse energy cascade and the Rhines scale, *J. Atmos. Sci.*, *64*, 3312–3327.
- Theiss, J. (2006), A generalized Rhines effect and storms on Jupiter, *Geophys. Res. Lett.*, *33*, L08809, doi:10.1029/2005GL025379.
- Vallis, G. K. (2006), *Atmospheric and Oceanic Fluid Dynamics: Fundamentals and Large-scale Circulation*, 745 pp., Cambridge Univ. Press, Cambridge, U. K.
- Vasavada, A. R., and A. P. Showman (2005), Jovian atmospheric dynamics: An update after Galileo and Cassini, *Rep. Prog. Phys.*, *68*, 1935–1996.
- Vasavada, A. R., S. M. Hörst, M. R. Kennedy, A. P. Ingersoll, C. C. Porco, A. D. D. Genio, and R. A. West (2006), Cassini imaging of Saturn: Southern hemisphere winds and vortices, *J. Geophys. Res.*, *111*, E05004, doi:10.1029/2005JE002563.

D. S. Choi and A. P. Showman, Department of Planetary Sciences, University of Arizona, 1629 E. University Blvd., Tucson, AZ 85721, USA. (dchoi@lpl.arizona.edu; showman@lpl.arizona.edu)

A. B. Penny, Department of Atmospheric Sciences, University of Arizona, 1118 E. Fourth St., Tucson, AZ 85721, USA. (penny@atmo.arizona.edu)